

Determining the Conditions for Dynamic Recrystallization in Hot Deformation of C–Mn–V Steels and the Effects of Cr and Mo Additions

Charles de Abreu MARTINS,¹⁾ Evgueni POLIAK,^{2)*} Leonardo Barbosa GODEFROID³⁾ and Nina FONSTEIN²⁾

1) ArcelorMittal Tubarão, Vitória, Espírito Santo, Brazil.

2) ArcelorMittal Global R&D, East Chicago, IN, USA.

3) Universidade Federal de Ouro Preto, Ouro Preto, Minas Gerais, Brazil.

(Received on July 19, 2013; accepted on August 26, 2013)

The refinement of microstructure and its homogeneity during controlled hot strip rolling is primarily achieved by controlling the austenite recrystallization before its transformation during accelerated cooling. The paper describes the methodology to determine the deformation conditions favorable for dynamic recrystallization (DRX). Using this methodology it becomes possible to delineate the conditions for post-deformation static and metadynamic recrystallization as well. The work is based on viscoplastic power law formalism applied to steady state flow within wide range of deformation temperatures and strain rates. Two equations of the same form but with different coefficients can be used depending on whether the steady state flow is controlled by dynamic recovery (DRV) or DRX. The transition from DRV- to DRX at the corresponding value of Zener-Hollomon parameter Z_T can be viewed as the demarcation between static and metadynamic recrystallization occurring after deformation. The approach is illustrated using low carbon Mn–V steel. Alloying with Cr and especially with Mo suppresses DRX and MDRX as manifested by increasing Z_T .

KEY WORDS: low alloy steels; hot deformation; dynamic recrystallization; dynamic recovery; power law.

1. Introduction

Controlled hot strip rolling of low carbon low alloyed steels aims at refining the microstructure to enhance mechanical properties of both as hot rolled strips and after further processing. The refinement of microstructure is primarily achieved by controlling the recrystallization of austenite before its transformation during accelerated run-out table cooling.^{1–3)} The recrystallization behavior of austenite during and after hot deformation operations is thus one of the key factors determining the hot rolling strategy and processing parameters.

In developing the strategy for controlled rolling it is important to keep in mind that partial recrystallization of hot rolled austenite prior to the beginning of its transformation is highly detrimental for the properties of steel products even after downstream processing. The type and kinetics of phase transformation in cooling of deformed austenite differ dramatically from those of recrystallized austenite.⁴⁾ When austenite is only partially recrystallized before transformation, the deformed and recrystallized portions transform into different phases and at different rates which results in highly variable microstructure and hence properties after cooling. This is further exacerbated by temperature, strain and strain rate variability within a bar and between bars typical for

industrial hot rolling. Because of these variations in processing parameters the partial recrystallization of austenite is practically uncontrollable. The induced variability of microstructure and hot band mechanical properties cannot be eliminated in cold rolling and is inevitably carried over into the annealing. Therefore, minimization of downstream non-uniformity of microstructure and properties to improve the final quality of steel sheet products requires obtaining more uniform and well controlled hot band microstructure, particularly by avoiding partial recrystallization of austenite during hot strip mill processing.

In hot rolling of austenite, the recrystallization of the following types is known to occur. First to mention is the dynamic recrystallization (DRX) during deformation in the roll bite. After deformation (*i.e.*, between the rolling passes and after existing the last finishing pass) the conventional static recrystallization (SRX) can take place if the strain in the preceding rolling passes has not been high enough to initiate DRX.⁵⁾ When strain is sufficient to ignite DRX, the metadynamic recrystallization (MDRX) occurs after deformation.⁶⁾ If DRX is incomplete then after deformation both SRX and MDRX can operate simultaneously: dynamically recrystallized portions of material continue to recrystallize metadynamically while the remaining portions can undergo SRX.⁶⁾

There is an important practical distinction between MDRX and SRX: the former starts immediately after deformation whereas certain time has to elapse before the onset

* Corresponding author: E-mail: evgueni.poliak@arcelormittal.com
DOI: <http://dx.doi.org/10.2355/isijinternational.54.227>

of SRX. In other words, SRX requires the so-called incubation time for initiation, while for MDRX the incubation time is zero.⁷⁾ Because of that, controlling the austenite recrystallization to prevent mixed non-uniform grain structure in hot rolled steel implies two important aspects. First, it is necessary either to avoid DRX during deformation (which eliminates MDRX between passes and after deformation) or, on the contrary, to ensure the completion of DRX. Second, the initiation of SRX can be suppressed by making the incubation time longer than the characteristic time periods of rolling process (interpass times, gap between the last pass exit and the beginning of transformation in accelerated cooling, *etc.*). Conversely, the completion of SRX can be achieved by the extending the time available for SRX after deformation. Thus, SRX control can be accomplished by adjusting the rolling speed so as to prevent SRX or, alternatively, to ensure its full completion before the onset of transformation. It is MDRX that is more harmful in terms of generating non-homogeneous grain structures in austenite, which is aggravated by lack of control over MDRX initiation because of the absence of the incubation time.

For these reasons, the first step in austenite recrystallization control is to define the processing conditions favorable for DRX and hence for MDRX. This would enable designing the hot rolling process as to avoid or facilitate the recrystallization of these types. The paper describes the methodology for determining the ranges of deformation conditions under which DRX can occur.

Steel chemistry has a profound impact on austenite recrystallization. Alloying with the elements known to slow down the initiation and progress of any kind of recrystallization can render better control over microstructure evolution in hot rolling. Another objective of the present work is to study the effects of chemical composition on the DRX and MDRX ranges of processing parameters for a number of C–Mn–V steels.

2. Experimental

The present work employed C–Mn–V steels with variable Cr or Mo content as shown in **Table 1**. Steels were laboratory melt and cast in 20 kg ingots. After cooling, the ingots were reheated at 1 250°C and hot rolled with the laboratory hot rolling mill to 20 mm thick plates. Portions of the plates were machined into standard cylindrical Ø 10 mm × 15 mm specimens for testing in uniaxial compression using Gleeble® 3500 thermomechanical simulator. Prior to testing the specimens were solution treated for 30 min at 1 250°C to dissolve possible precipitates in hot rolled plates and thus to simulate the condition of the austenite after slab reheating in industrial hot rolling. During the tests, the specimens were reheated at 9°C/sec to 1 100°C and soaked at this temperature for 30 sec to ensure full austenitization but at the same time to prevent significant grain growth. This was followed by cooling of the specimens at 5°C/sec to test temperatures of 750–1 050°C varied in 50°C increments and soaking for 60 sec before deformation. Since the equilibrium A_{e3} transformation temperatures for the studied steels are relatively high (*cf.* Table 1) the dilatometry measure-

Table 1. Chemical compositions and austenite-to-ferrite transformation temperatures of the studied steels.

	Steel 1	Steel 2	Steel 3	Steel 4	Steel 5	Steel 6
C	0.12	0.12	0.11	0.12	0.12	0.12
Mn	1.69	1.71	1.70	1.69	1.70	1.72
P	0.008	0.009	0.009	0.009	0.009	0.009
S	0.001	0.001	0.001	0.001	0.001	0.002
Alloy content, mass%						
Si	0.307	0.309	0.315	0.311	0.308	0.321
Al	0.035	0.031	0.031	0.03	0.04	0.041
Mo	–	–	–	–	0.248	0.501
Cr	0.251	0.502	0.762	1.016	–	–
V	0.193	0.208	0.202	0.204	0.198	0.212
N	0.0047	0.0057	0.0062	0.0060	0.0059	0.0059
A_{e3}^{ortho}	833	830	830	825	842	848
A_{e3}^{para}	805	800	801	796	812	817
$A_{r3}^{(5)}$	610	601	593	536	582	553
$A_{r3}^{(2)}$	678	669	673	663	642	601

A_{e3}^{ortho} , A_{e3}^{para} – calculated, Thermocalc 3.0.1

$A_{r3}^{(5)}$, $A_{r3}^{(2)}$ – measured by dilatometry after austenitization at 1 100°C for 30 sec and subsequent cooling at 5 and 2°C/sec, respectively.

ments of A_{r3} temperatures after reheating at 1 100°C and cooling at various rates were performed using MMC dilatometer[†] to make sure that austenite transformation did not take place before and during deformation in Gleeble. As shown in Table 1, the A_{r3} temperatures pertinent to the described thermal profile of the compression tests are significantly lower than the test temperatures.

After soaking at test temperature, the specimens were isothermally compressed in one hit up to true strain of about 0.8 (55% height reduction) at constant strain rates of 0.1, 1.0, and 10.0 sec⁻¹. The “load – stroke” machine data were converted into the “true stress – true strain” flow curves using constant volume and uniform deformation assumptions.

3. Results and Discussion

3.1. Stress – Strain Curves

The stress - strain curves generated in Gleeble compression tests are exemplified in **Fig. 1**. They are typical for low carbon low alloyed steels. The full set of curves is shown only for the least alloyed Steel 1 (Fig. 1(a)). For Steel 4 with the highest Cr content (Fig. 1(b)) and Steel 6 with the highest Mo content (Fig. 1(c)) only the curves for one strain rate are displayed to better illustrate the derivations that follow. The flow curves for other studied steels are qualitatively similar to those in Fig. 1.

At low test temperatures the stress - strain curves do not reveal any signs either of deformation in austenite + ferrite range or a dynamic $\gamma \rightarrow \alpha$ -transformation, both of which would manifest themselves in flow stress drops and continuous softening after stress peak.^{8,9)} The absence of such manifestations may be regarded as additional confirmation that the specimens were indeed deformed in single phase

[†]The detailed results of dilatometry studies intended for development of the hot strip mill run-out table cooling strategies are to be published separately.

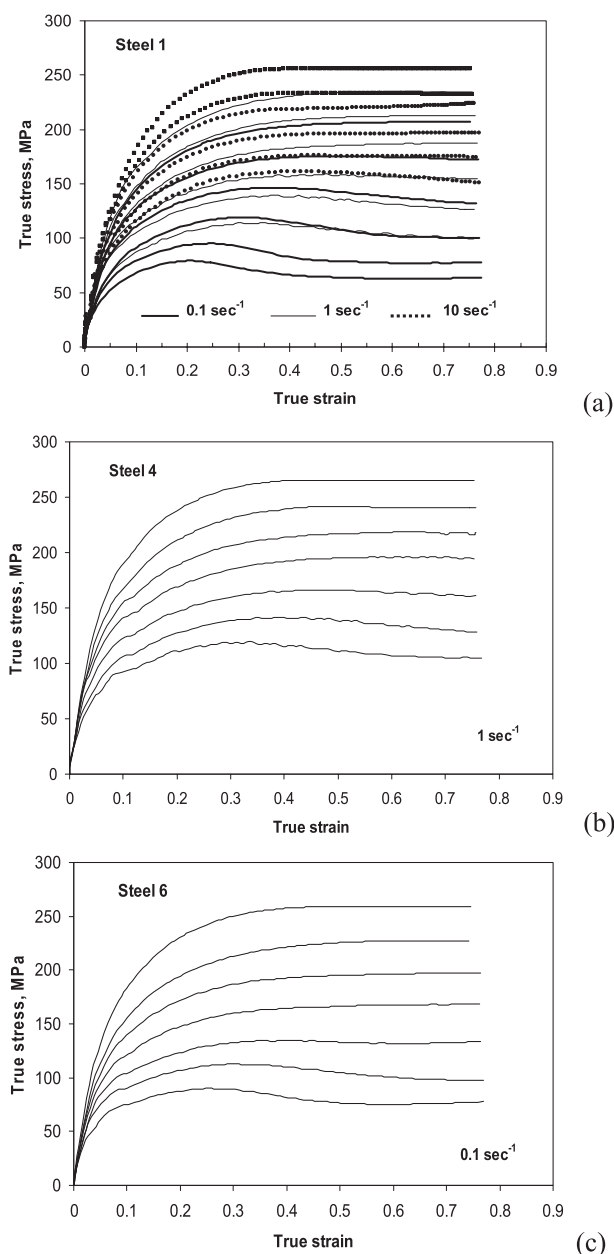


Fig. 1. Examples of stress-strain flow curves. Test temperatures vary in 50°C increments from top (750°C) to bottom (1 050°C) curves: (a) – Steel 1, (b) – Steel 4, (c) – Steel 6.

austenite.

Based on their shape the flow curves can be classified into the following three categories. First, there are curves with typical DRX shape exhibiting pronounced stress peaks and steady state flow. These DRX-type curves correspond to higher test temperatures and lower strain rates. In contrast, the stress-strain curves obtained at lower temperatures and higher strain rates show no stress peaks but only the steady state flow. Such curves are traditionally associated with dynamic recovery (DRV) only and can therefore be referred to as of the DRV-type*. Finally, at intermediate temperatures, several curves can be identified in Fig. 1 having what can be called a “transient”-type shape with poorly pro-

nounced very broad low stress peaks barely distinguishable from the steady state.

The occurrence of MDRX can be anticipated after deformation under the conditions at which the DRX-type flow curves are observed. In case of DRV-type flow curves, SRX is the only expectable post-deformation recrystallization.

Steel chemistry within the studied ranges of composition does not affect the shape of the flow curves. For all steels, the above three types of stress-strain curves were detected. It should be noted that with Cr additions of up to 1 wt.% the flow stress slightly increases. Alloying with Mo raises the overall level of flow stress more appreciably.

3.2. Effects of Strain Rate and Temperature on Steady State Stress

In this Section, the approach to analyzing the flow stress is outlined with the objective to determining the deformation conditions favorable for DRX and hence for MDRX. The details are illustrated using the test data for Steel 1. The results for other steels and the effects of alloying are discussed in the next Section.

The present analysis employs the steady state stresses σ_s only. In agreement with numerous experimental observations of isothermal constant strain rate deformation, the high temperature steady state flow stress and microstructure are determined only by the applied strain rate and temperature.¹¹⁾ Thus, the considerations based on steady state stresses allow avoiding discrepancies stemming from possible effects of microstructure prior to deformation and particularly those of the initial austenite grain size as, for example, in the case of the peak stresses.¹¹⁾ Also it is worth recalling that in hot deformation of austenite the stress peaks are observed only when DRX takes place. Since DRX is known to begin before the stress peak is reached^{11–16)} the microstructure at stress peak is in fact a mixture of recrystallized and non-recrystallized austenite. Such mixed microstructure leads to highly unstable hardening behavior: slight increase in strain beyond the peak induces rapid and drastic changes in flow stress and strain hardening rate. There is no physical analogy to such behavior in case of DRV.

In the steady state deformation, on the other hand, the microstructure is stable and independent of the initial microstructure. The flow stress is determined solely by the controlling softening mechanism and is invariant with increasing strain as long as the temperature and strain rate are maintained constant and the deformation remains uniform. From this viewpoint, a unified analysis of DRX and DRV controlled flow is only viable for the steady states.

The viscoplastic power law for the steady state flow is now assumed to hold for the entire range of studied deformation conditions (absolute temperatures T and strain rates $\dot{\epsilon}$). The effects of T and $\dot{\epsilon}$ on the flow stress can then be evaluated by plotting the experimentally obtained values of $\ln \sigma_s$ against reciprocal absolute temperature for each strain rate. These plots for Steel 1 are displayed in Fig. 2. As expected, the steady state stress increases with decreasing test temperature and increasing strain rate.

*Stress-strain curves with the shape similar to that of the DRV-type are also observed in case of continuous DRX (CDRX) predominantly in high stacking fault energy materials, e.g., Al.¹⁰⁾ However, the initiation of CDRX requires high strains ($\epsilon \sim 2-4$)¹⁰⁾ that far exceed the strain range applied in compression tests of this work. Therefore, CDRX is excluded from the present considerations.

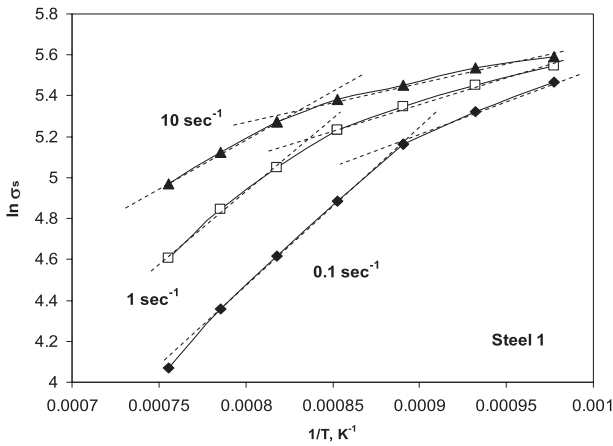


Fig. 2. Temperature and strain rate dependences of steady state stress, Steel 1.

The least squares fitting reveals that each $\ln \sigma_s - 1/T$ plot is best approximated by two linear segments (Fig. 2) indicating two distinct steady state behaviors. Two families of linear segments are readily identifiable in Fig. 2: at higher temperatures (lower $1/T$), $\ln \sigma_s$ follow straight lines with steeper slopes while at higher $1/T$ the slopes are essentially lower. Within each family the $\ln \sigma_s - 1/T$ plots are not parallel, their slopes decrease as the strain rate is increased.

With reference to Fig. 1(a), it can be noticed that for each strain rate the two linear segments in Fig. 2 correlate with the shape of the flow curves. The $\ln \sigma_s - \text{low } 1/T$ linear segments (higher slope) correspond to the DRX-type flow curves, *i.e.* these segments pertain to the temperatures and strain rates of the occurrence of DRX. The higher $1/T$ segments correspond to the DRV-type curves, *i.e.*, to the ranges of deformation conditions under which the steady state flow is controlled by DRV, and not by DRX.

At given strain rate, the flow curves with the transient-type shape are observed at temperatures at which the slope of linear segments changes sharply. In this temperature range, $\ln \sigma_s$ can be equally well attributed to either of the two linear segments. Noteworthy that the values of $\ln \sigma_s$ within the temperature range of the transition exhibit weak strain rate dependence.

Naturally, each linear segment in Fig. 2 can be described by the equation

$$\ln \sigma_s = \frac{q}{T} + a_\sigma, \dots\dots\dots (1)$$

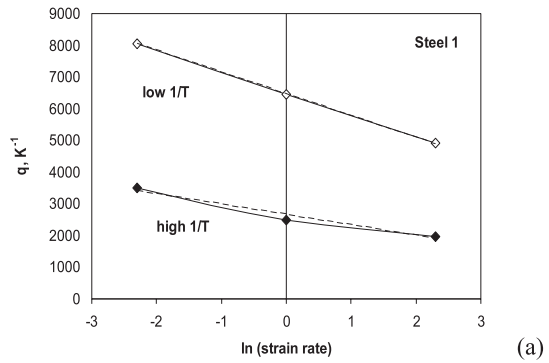
where q is the slope of the given segment (at given strain rate) and a_σ is the intercept. The values of q and a_σ for the two families of linear segments are plotted in Fig. 3 as the functions of $\ln \dot{\epsilon}$. These plots are also fairly linear so that these coefficients can be presented as

$$q = q_0 + a_q \ln \dot{\epsilon} \dots\dots\dots (2)$$

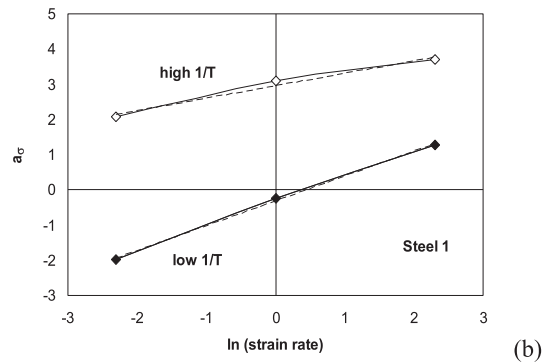
$$a_\sigma = a_{\sigma 0} + b \ln \dot{\epsilon} \dots\dots\dots (3)$$

where q_0 and $a_{\sigma 0}$ are the values of q and a_σ at $\dot{\epsilon} = 1 \text{ sec}^{-1}$, respectively. Combination of Eqs. (1)–(3) yields the equation

$$\ln \sigma_s = \left(q_0 + a_q \ln \dot{\epsilon} \right) \frac{1}{T} + a_{\sigma 0} + b \ln \dot{\epsilon}. \dots\dots\dots (4)$$



(a)



(b)

Fig. 3. Strain rate dependences of coefficients q (a) and a_σ (b) in Eq. (1).

Partial differentiation of Eq. (4) with respect to $\ln \dot{\epsilon}$ allows determining the strain rate sensitivity of the steady state stress,

$$m = \left. \frac{\partial \ln \sigma_s}{\partial \ln \dot{\epsilon}} \right|_T,$$

which is equal to

$$m = a_q \frac{1}{T} + b \dots\dots\dots (5)$$

if q_0 , a_q , $a_{\sigma 0}$ and b are independent of strain rate. On the other hand, partial differentiation of Eq. (4) with respect to $1/T$ gives the temperature sensitivity of the steady state stress:

$$q = \left. \frac{\partial \ln \sigma_s}{\partial (1/T)} \right|_{\dot{\epsilon}}$$

From Eqs. (2) and (4) the temperature sensitivity of stress is

$$q = q_0 + a_q \ln \dot{\epsilon}. \dots\dots\dots (6)$$

which is identical to Eq. (2) if q_0 , a_q , $a_{\sigma 0}$ and b are independent of temperature. As suggested by the experimental data in Figs. 2 and 3, for each family of linear segments the coefficients q_0 , a_q and b can be indeed considered constant. Then the strain rate sensitivity of stress, Eq. (5), appears to be only the function of temperature and the temperature sensitivity of stress, Eq. (6), is a function of strain rate only. By denoting

$$a_{\sigma 0} = \ln A,$$

Eq. (4) can be rewritten in two equivalent formulations of the power-law viscoplastic constitutive relationships:¹⁶⁾

$$\sigma_s(\dot{\epsilon}, T) = A \dot{\epsilon}^b \exp \left(\frac{q_0 + a_q \ln \dot{\epsilon}}{T} \right) \dots\dots\dots (7-1)$$

or

$$\sigma_s(\dot{\epsilon}, T) = A\dot{\epsilon}^{(b+a_q/T)} \exp\left(\frac{q_0}{T}\right) \dots\dots\dots (7-2)$$

where A is a scaling constant and either of the terms $A\exp(q_0 + a_q \ln \dot{\epsilon} / T)$ or $A\exp(q_0/T)$ is a viscosity-like parameter presented in the form of the Arrhenius law. Both of Eqs. (7) apply to the two families of linear segments in Fig. 2.

With numerical values of the empirical coefficients q_0 , a_q and b for Steel 1 computed from Fig. 2, the strain rate and temperature sensitivities of the steady state stress, Eqs. (5) and (6), can be respectively expressed as

$$\begin{aligned} m^{DRX} &= -684/T + 0.707 ; m^{DRV} = -331/T + 0.354 \\ q^{DRX} &= 6835 - 684 \ln \dot{\epsilon} ; q^{DRV} = 2652 - 331 \ln \dot{\epsilon} \end{aligned} \dots\dots\dots (8)$$

where the subscripts DRX and DRV refer to the low – and high $1/T$ ranges in Fig. 2, respectively, or, equivalently, to the DRX- and DRV type flow curves in Fig. 1(a), respectively.

As follows from Eqs. (8), at given strain rate the temperature sensitivity of steady state stress is higher in case of DRX, $q^{DRX} > q^{DRV}$. Also, at given temperature the strain rate sensitivity of stress is higher for DRX, $m^{DRX} > m^{DRV}$. The transition from DRV controlled to DRX controlled steady state flow is accompanied by increase in both strain rate and temperature sensitivities of the steady state stress.

At the DRV \leftrightarrow DRX transition

$$\sigma_s^{DRV} = \sigma_s^{DRX}.$$

With Eq. (4) and using the linear combinations of the coefficients in Eqs. (1)–(3) it becomes possible to determine the strain rate $\dot{\epsilon}_t$, at which transition takes place at the given temperature, or, alternatively, to determine the temperature T_t , at which the transition occurs at given strain rate. When $T < T_t$, the flow stress never becomes high enough to initiate DRX at the given strain rate. In other words, at $T < T_t$, DRX can never take place at given strain rate regardless of the applied strain. As follows from Fig. 2, the transition temperature T_t is higher the higher is the strain rate.

On the other hand, when $\dot{\epsilon} > \dot{\epsilon}_t$ the flow stress is also never high enough to ignite DRX at given temperature and so DRX can never be expected to occur, again irrespective of the applied strain. The data in Fig. 2 indicate that the transition strain rate $\dot{\epsilon}_t$ is higher the higher is the deformation temperature.

Thus, both $\dot{\epsilon}_t$ ($T = \text{const}$) and T_t ($\dot{\epsilon} = \text{const}$) delineate the ranges of the occurrence of DRX. Under favorable conditions, *i.e.*, at $T > T_t$ and/or $\dot{\epsilon} < \dot{\epsilon}_t$, DRX can only start when the critical strain for the onset of DRX is reached. When strain rates or temperatures do not favor DRX ($T < T_t$, $\dot{\epsilon} > \dot{\epsilon}_t$) the DRX critical strain can never be reached during deformation.

The presented experimental evidence of coupling between the DRX \leftrightarrow DRV transition temperature T_t and strain rate $\dot{\epsilon}_t$ points at the possibility to describe this transition using the Zener-Hollomon parameter (temperature compensated strain rate):

$$Z = \dot{\epsilon} \exp(Q_{def}/RT) \dots\dots\dots (9)$$

where R is the universal gas constant and Q_{def} is the apparent activation energy of deformation. In terms of Z the power law equation has the form^{17,18)}

$$\sigma_s = A'Z^n. \dots\dots\dots (10)$$

This formulation implies that the coefficients A' , n and Q_{def} remain constant with reasonable accuracy.

Putting $A' = A$ and using Eq. (4), the relationship between σ_s and Z can be rewritten as

$$n \ln Z = \ln \sigma_s - \ln A = (q_0 + a_q \ln \dot{\epsilon}) \frac{1}{T} + b \ln \dot{\epsilon} \dots\dots (11)$$

As shown above, the coefficients A , q_0 , a_q and b remain constant as long as the steady state flow is controlled either by DRV or DRX, *i.e.* for a single family of linear segments in Fig. 2. The DRX \leftrightarrow DRV transition is described by discontinuous change in A , q_0 , a_q and b at the temperature and/or strain rate of transition or, equivalently, by change in strain rate and temperature sensitivities of the steady state stress. Consequently, at the DRX \leftrightarrow DRV transition the coefficients A' , n and Q_{def} must change discontinuously as well. That is, the coefficients in Eq. (10) should be different depending on whether the steady state flow is controlled by DRV or by DRX. Accordingly, the parameter Z should be defined separately for DRX and DRV domains.

By definition,

$$n = \frac{\partial \ln \sigma_s}{\partial \ln \dot{\epsilon}} \Big|_T = m$$

and

$$Q_{def} = \frac{R}{m} \left[\frac{\partial \ln \sigma_s}{\partial (1/T)} \right]_{\dot{\epsilon}} = \frac{R}{m} q$$

Within the framework of the present approach the strain rate sensitivity of steady state stress m and temperature sensitivity q are not constant even for a single family of linear segments in Fig. 2 but vary with temperature and strain rate, respectively, *cf.* Eqs. (5) and (6). Then n and Q_{def} should not be in fact constant for a family of linear segments. This, however, does not mean that the power law in form of Eq. (10) cannot be applied.¹⁶⁾ Following traditional treatments, the coefficient n can be taken equal to the average strain rate sensitivity of stress over the temperature range at which a single dynamic softening mechanism operates,¹⁷⁾ $n = \bar{m}$. The apparent activation energy Q_{def} can be expressed through the temperature sensitivity of stress averaged over the range of $\ln \dot{\epsilon}$. In this study $\overline{\ln \dot{\epsilon}} = 0$, so that Q_{def} can be defined as

$$Q_{def} = \frac{R}{\bar{m}} q_0 \dots\dots\dots (12)$$

For the two families of linear segments in Fig. 2, $\bar{m}^{DRX} = n^{DRX} = 0.16$, $\bar{m}^{DRV} = n^{DRV} = 0.08$, $Q_{def}^{DRX} = 355$ kJ/mol, $Q_{def}^{DRV} = 275$ kJ/mol. These values are consistent with the general view that DRV and DRX are associated with different apparent activation energies. When the steady state flow is controlled by DRV the activation energy Q_{def} is comparable with the activation energy for iron self-diffusion in austenite (284 kJ/mol¹⁹⁾) while in case of DRX the activation energy Q_{def} is significantly higher.^{20,21)}

Figure 4 shows the dependences of steady state flow

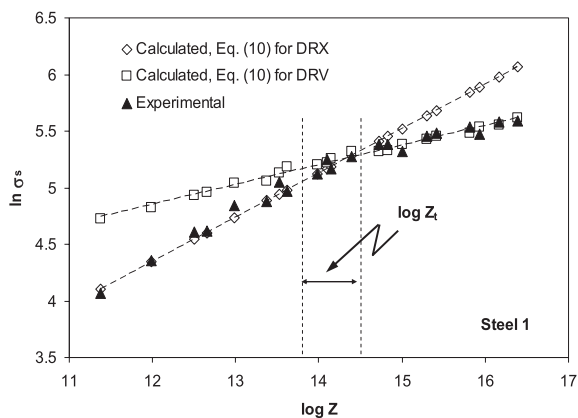


Fig. 4. Dependences of experimental and calculated steady state flow stresses on Zener-Hollomon parameter with Z computed separately for DRV and DRX using the respective values of Q_{def} .

stresses, both obtained experimentally and calculated with Eq. (10), on Zener-Hollomon parameter. The latter was computed separately for DRV and DRX using the respective values of Q_{def} . The flow stresses were then calculated with the corresponding values of n . The two calculated $\ln \sigma_s - \log Z$ plots intersect at Z_i . At $Z < Z_i$ the experimental data align quite well with $\ln \sigma_s$ computed using Q_{def}^{DRX} and n^{DRX} . On the other hand, at $Z > Z_i$ the experimental $\ln \sigma_s$ match the calculations that employ Q_{def}^{DRV} and n^{DRV} . Change in controlling mechanism is manifested by abrupt change in the slope of experimental $\ln \sigma_s - \log Z$ plot at Z_i . That is, Fig. 4 shows that the dominant softening mechanism is determined by the lowest level of the steady state stress.

Although the change in flow controlling mechanism can be attributed to certain transition value of Zener-Hollomon parameter Z_i , the actual DRX \leftrightarrow DRV transition spans over some range of Z_i , Fig. 4. Most likely this range pertains to the deformation conditions under which the DRX and the DRV steady state stresses are close to each other. Within the range of Z_i the flow curves of the transient type are observed. The range of Z_i also explains slight variation in transition stress with strain rate (or temperature) mentioned earlier with reference to Fig. 2.

It is also worth noting that in part the scatter in Z_i can be contributed by purely mechanical factors, *i.e.*, by low accuracy of maintaining constant strain rate of 10 sec^{-1} . At this strain rate the total time of deformation is about 0.08 sec, which is comparable with the time for ram acceleration and deceleration in Gleeble[®] 3500 machine so that in such tests the strain rate is not in fact constant.

Nonetheless, Z_i can be viewed as the demarcation between DRX and DRV and hence as lower bound for post-deformation MDRX, similarly to T_i and $\dot{\epsilon}_i$.

3.3. Effects of Alloying

The procedures and analysis described in the previous Section and illustrated for Steel 1 were applied to all steels studied in this work. The related effects of steel chemistry are now addressed. As already noted, alloying with up to 1% Cr does not significantly impact the overall level of flow stress and the steady state stress in particular (Fig. 5) although the latter tends to grow slightly with increasing Cr

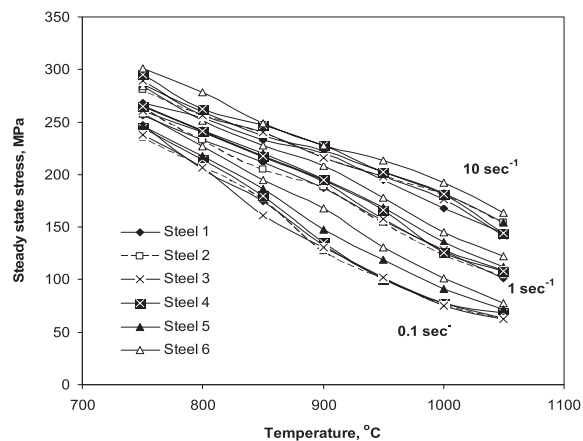


Fig. 5. Effects of temperature, strain rate and steel composition on the steady state flow stresses.

content due to solid solution strengthening of austenite. Alloying with Mo induces more appreciable strengthening especially at lower strain rates and higher temperatures, Fig. 5.

The plots in Fig. 5 also do not indicate the occurrence of phase transformation in the entire temperature range employed here as no stress decrease with decreasing temperature is observed, as should have been had the transformation taken place.⁹⁾

Temperature and strain rate dependences of the steady state flow stresses for Steels 2–6 are displayed in Fig. 6 in the form of $\ln \sigma_s - 1/T$ plots. These are similar to the plots shown in Fig. 2 for Steel 1. In all cases, two linear segments can be identified corresponding to the DRX-type and DRV-type flow curves.

The DRV – DRX transition temperatures T_i determined from the plots in Fig. 6 are displayed in Fig. 7 as functions of strain rate and steel chemistry. As was observed in case of Steel 1, for all other steels T_i increases as the strain rate is increased.

Addition of 0.25 to 0.75% Cr raises the transition temperature by some 20–40°C. The effect of alloying with Cr is more pronounced at higher strain rate. However, with increasing of Cr content up to 1% the transition temperature drops to the same level as for low Cr steel (0.25% Cr), this behavior is observed at all strain rates. These variations indicate that small additions of Cr tend to slightly hinder DRX but at higher Cr content this effect disappears which can indicate the change in the way chromium influences the deformation behavior of austenite. At small Cr concentrations, a weak solid solution strengthening may determine the deformation behavior of austenite while at higher concentration (around 1 mass%) the decrease in the stacking fault energy of austenite due to presence of Cr may start to dominate thus facilitating recrystallization.

Alloying with Mo strongly inhibits DRX as manifested by significantly higher transition temperatures than in case of alloying with Cr, Fig. 7. Even low Mo concentration is quite efficient in suppressing DRX and this effect becomes stronger with higher Mo content irrespective of the strain rate, Fig. 8. Suppressing of austenite recrystallization by molybdenum detected in this study is consistent with findings of other researchers.^{5,22,23)}

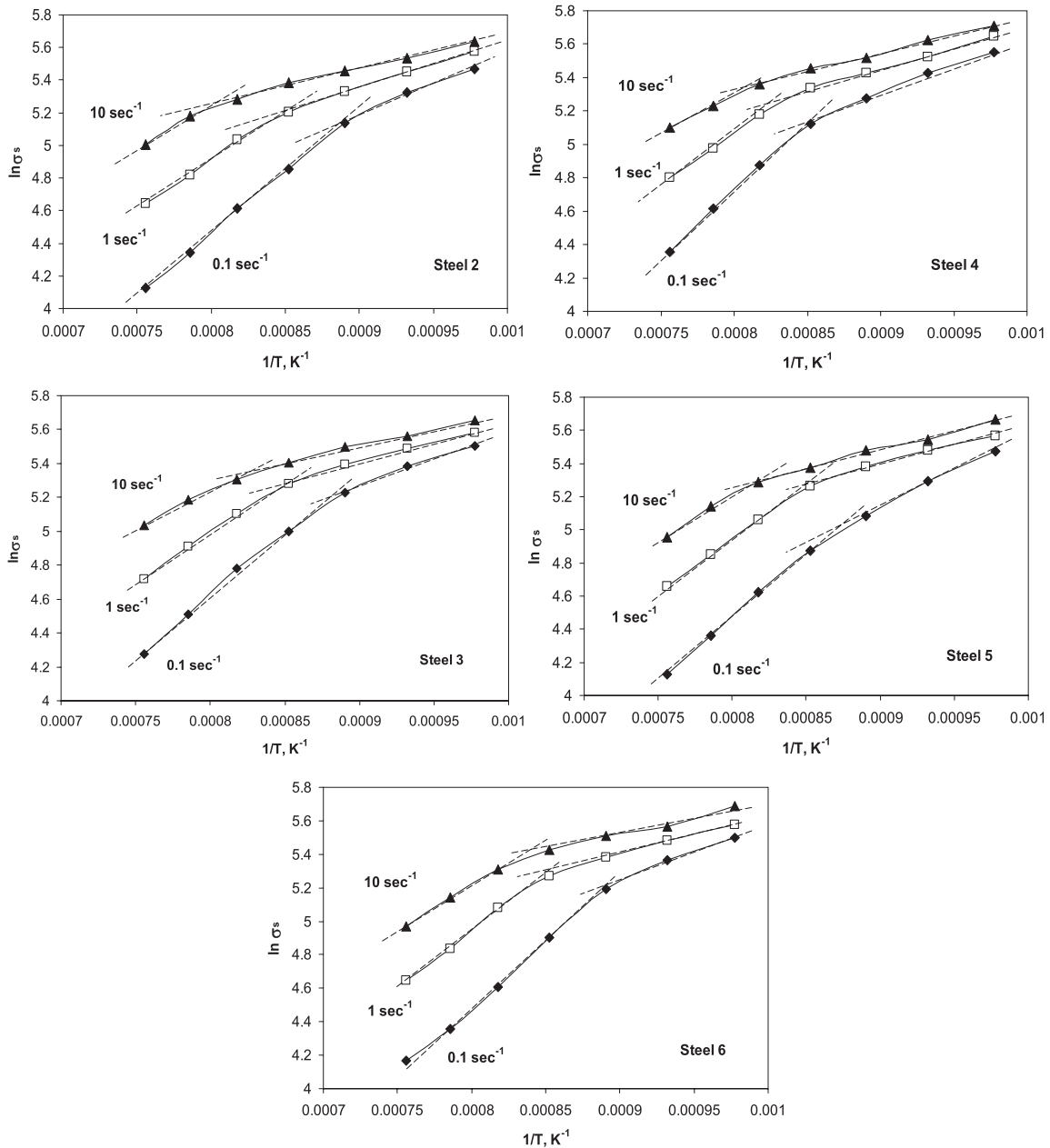


Fig. 6. Linearized temperature and strain rate dependences of $\ln \sigma_s$ for Steels 2–6.

3.4. Practical Implications

The results presented above can be directly applied to controlled hot rolling process design aimed to maximize the homogeneity of austenite grain structure. To avoid DRX in a given rolling pass (so that to avoid immediate MRDX after the pass), the bar temperature must be below the transition temperature T_i . In particular, if DRX has to be avoided in the entire finishing rolling sequence the finishing mill entry temperature must be lower than T_i . In typical hot strip mills the finishing entry temperatures are about 1000–1050°C and the first pass strain rates are close to 10 sec^{-1} . As follows from Figs. 7 and 8, under such conditions all of the steels studied here are prone to DRX which indicates that DRX will take place in the first finishing pass if the reduction in this pass exceeds the DRX critical strain. In this case MDRX will start immediately upon the exit from the roll bite. As the result, highly non-homogeneous austenite grain structure will emerge that can be further carried over

through the entire finishing mill. The likelihood of such an unfortunate scenario is much less for Steel 6 with 0.5 wt.% Mo since this composition has the highest stability against DRX and MDRX as manifested by the highest transition temperature at 10 sec^{-1} (Figs. 7 and 8).

The possible countermeasures to prevent generation of mixed austenite grain microstructure by DRX and MDRX can be seen in lowering the finishing mill entry temperature and/or increasing the entry speed and hence the strain rate. This way both processing parameters can be brought outside the DRX domain. It is also possible to lower the reduction in the first pass making it below DRX critical strain. All of these measures, however, may not be viable and readily applicable. Lowering the entry temperature and/or increasing the rolling speed lead to higher flow stresses and hence to higher roll separation forces. Redrafting the mill as to reduce the first pass reduction may also be harmful since in this case more draft should be taken in downstream passes

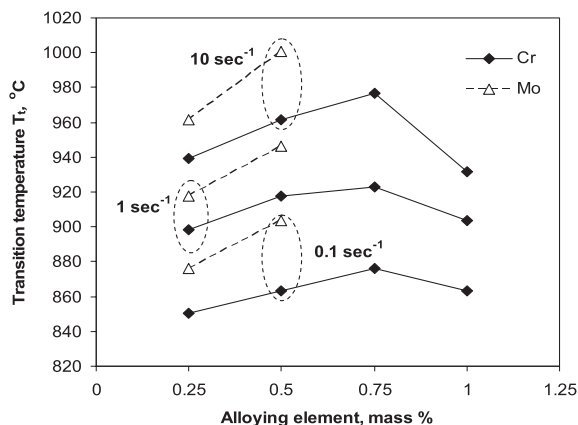


Fig. 7. Effects of steel chemistry and strain rate on DRV ↔ DRX transition temperature.

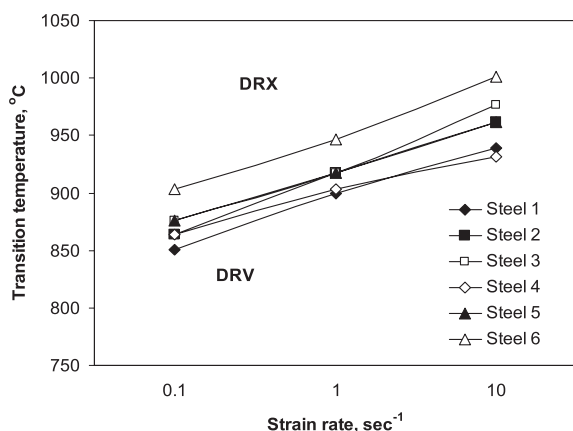


Fig. 8. Schematic map of steady state flow controlling mechanisms for the studied steel compositions.

where the roll force can also increase because of higher reductions and higher flow stresses due to lower temperatures of the strip.

An alternative strategy can imply raising the finishing mill entry temperature above T_t , reducing the finishing mill entry speed and/or applying heavy reduction in the first pass to ensure the highest possible extent of the progress of DRX. In any case, however, the hot rolling strategy should be carefully selected with account for product dimensions, configuration and capabilities of the particular hot strip mill.

4. Conclusions

(1) Hot compression tests of low carbon low alloy steels at temperatures of 750–1050°C and strain rates of 0.1–10.0 sec^{-1} indicate that the plastic flow is controlled either by DRV or DRX depending on the deformation temperature and strain rate. The viscoplastic power law formalism can be applied to steady state flow within the above ranges of deformation conditions. DRV- and DRX controlled steady state stresses can be described by equations of the same form but with different coefficients.

(2) As the deformation temperature is increased at fixed

strain rate, the transition from DRV- to DRX controlled plastic flow occurs at certain temperature T_t ; similarly, at constant temperature the transition from DRV- to DRX flow occurs at certain strain rate $\dot{\epsilon}_t$. More generally, this transition can be described by the corresponding value of Zener-Hollomon parameter Z_t . T_t is higher the higher is the strain rate; $\dot{\epsilon}_t$ is higher the higher the deformation temperature.

(3) The transition from DRV- to DRX controlled flow when deformation temperature and/or strain rate are varied can be viewed as the demarcation between static and meta-dynamic recrystallization occurring after deformation.

(4) Alloying of 0.12% C–1.7% Mn steel with up to 0.75% Cr hinders DRX as manifested by higher DRX ↔ DRV transition temperature. However, T_t decreases with further additions of chromium. Alloying with up to 0.5% Mo efficiently suppresses DRX; the effect of molybdenum is far stronger than that of chromium.

Acknowledgements

The permission for publication of this paper from ArcelorMittal is acknowledged with deep gratitude. The authors are indebted to Dr. D. Bhattacharya of ArcelorMittal Global R&D for his encouragement and support of this work. They are also thankful to Prof. F. Boratto of Pontificia Universidade Católica de Minas Gerais for fruitful and stimulating discussions.

REFERENCES

- 1) J. J. Jonas: *ISIJ Int.*, **40** (2000), 731.
- 2) J. J. Jonas: Proc. of 2nd Int. Conf. Thermomechanical Processing TMP 2004. Liege, Belgium, Verlag Stahleisen GmbH, Dusseldorf, (2004), 35.
- 3) M. Venkatraman and T. Venugopalan: Proc. of 2nd Int. Conf. Thermomechanical Processing TMP 2004. Liege, Belgium, Verlag Stahleisen GmbH, Dusseldorf, (2004), 99.
- 4) R. H. Larn and J. R. Yang: *Mater. Sci. Eng. A*, **A278** (2000), 278.
- 5) C. Roucoules, P. D. Hodgson, S. Yue and J. J. Jonas: *Metall. Mater. Trans.*, **25A** (1994), 389.
- 6) J. H. Bianchi and L. P. Karjalainen: *J. Mater. Process. Technol.*, **160** (2005), 267.
- 7) P. D. Hodgson: Proc. of Int. Conf. THERMEC-97, ed. by T. Chandra and T. Sakai, Minerals, Metals and Materials Society, Warrendale, PA, (1997), 121.
- 8) J. K. Choi, D.-H. Seo, J. S. Lee and W. Y. Choo: *ISIJ Int.*, **43** (2003), 746.
- 9) N. K. Park, A. Shibata, D. Terada and N. Tsuji: *Acta Mater.*, **61** (2013), 163.
- 10) S. Gourdet and F. Montheillet: *Mater. Sci. Eng. A*, **A283** (2000), 274.
- 11) T. Sakai and J. J. Jonas: *Acta Metall.*, **32** (1984), 189.
- 12) N. D. Ryan and H. J. McQueen: *Can. Metall. Q.*, **29** (1990), 147.
- 13) E. I. Poliak and J. J. Jonas: *Acta Metall. Mater.*, **44** (1996), 127.
- 14) S. B. Davenport, N. J. Silk, C. N. Sparks and C. M. Sellars: *Mater. Sci. Technol.*, **16** (2000), 539.
- 15) A. I. Fernandez, P. Uranga, B. Lopez and J. M. Rodriguez-Ibabe: *Mater. Sci. Eng.*, **A361** (2003), 367.
- 16) F. Montheillet and J. J. Jonas: *Metall. Mater. Trans. A*, **27A** (1996), 3346.
- 17) H. J. McQueen and N. D. Ryan: *Mater. Sci. Eng. A*, **A322** (2002), 43.
- 18) H. Mirzadeh, J. M. Cabrera and A. Najafzadeh: *Acta Mater.*, **59** (2011), 6441.
- 19) Smithells Metal Reference Book, 7th ed., Butterworth-Heinemann Ltd., Oxford, UK, (1992).
- 20) J. J. Jonas, C. M. Sellars and W. J. McG. Tegart: *Int. Metall. Rev.*, **14** (1969), 1.
- 21) N. D. Ryan and H. J. McQueen: *J. Mech. Working Technol.*, **12** (1986), 279.
- 22) H. L. Andrade, M. G. Akben and J. J. Jonas: *Metall. Trans.*, **14A** (1983), 1967.
- 23) S. F. Medina and J. E. Mancilla: *ISIJ Int.*, **36** (1996), 1070.